The Astrophysical Journal, 882:146 (12pp), 2019 September 10 https://doi.org/10.3847/1538-4357/ab3348

The Thermal Force in Astrophysical Plasmas: Current Free Coulomb Friction

J. D. Scudder
Department of Physics and Astronomy, University of Iowa, Iowa City, IA 52442, USA
Received 2019 May 24; revised 2019 July 2; accepted 2019 July 16; published 2019 September 11

Abstract

The *thermal force* (TF) is an exchange force mediated by Coulomb collisions between electrons and ions in a heat-conducting astrophysical plasma, is one of three, non-inertial, balancing terms in the parallel component of the generalized Ohm's law, and is magnetic field aligned with a size that scales with and is parallel to the dimensionless heat flux. The TF (i) increases the size of $E_{\|}$ above that implied by the electron pressure divergence; (ii) deepens the electrostatic trap for electrons about the Sun; (iii) strengthens the electron kurtosis and skewness, further levitating ions out of their gravitational well, (iv) constrains the heat flow in a plasma where parallel currents are preempted; and (v) is shown to be directly measurable using the full electron velocity distribution function above and below thermal energies. (vi) The usually ignored TF modifies all species internal energy equations; it enhances the rate of conduction cooling by the electrons, increases the ion entropy, and forestalls adiabatic behavior. Using estimates at 1 au this effect is especially strong in the higher speed wind $U > 400\,\mathrm{km\,s^{-1}}$ regime. (vii) On rather general grounds any physical heat transport is accompanied by an underlying TF; in almost all known cases of modeling astrophysical plasmas this dependence is ignored or demonstrably incorrect. It follows that attempts to predict species specific pressures without inclusion of the TF is *futile*.

Key words: conduction – magnetohydrodynamics (MHD) – plasmas – solar wind – stars: coronae

1. The Physics of the Thermal Force

The *thermal force* (TF) is a friction unique to plasmas and Coulomb collisions in high-temperature astrophysical plasmas where heat flow is virtually unavoidable. The TF remains nonzero even when the center of mass for all species are matched, as assumed when making the $\boldsymbol{J}_{\|} = 0$ idealization for plasma fluid modeling of solar wind and commonly for other astrophysical plasma modeling. It was explicitly identified in Braginksii's seminal paper (Braginskii 1965), but its role in the literature dates back to 1953 when its effects were included in the Spitzer & Härm (1953) determination of the heat diffusivity coefficient (Rossi & Olbert 1970; Ferziger & Kaper 1972; Balescu 1988; Fitzpatrick 2014). While the Spitzer–Härm derivation included the (unnamed) TF in its development, the resulting closure was limited to (i) small magnetically aligned ($\hat{\boldsymbol{b}}$) pressure Knudsen numbers

$$\mathbb{K}_P \equiv -\hat{\boldsymbol{b}} \cdot \nabla \ln P_e \lambda_{\mathrm{mfp}}, \tag{1}$$

assumed infinitesimal, and (ii) for systems with vanishing field-aligned forces such as pressure gradients or gravity (Spitzer 1965; Balescu 1988). While there have been attempts to include TF and field-aligned forces, they have only been carried out for the infinitesimal $\mathbb{K}_P$ regimes (Ferziger & Kaper 1972; Balescu 1988), which are *not* generally appropriate for most astrophysical plasmas with finite steady-state pressure Knudsen numbers. Until now the TF's role seems to have been overlooked when heat relations are adopted for the solar wind and coronal modeling (e.g., Breech et al. 2009; Cranmer et al. 2009), where finite $\mathbb{K}_P$ is always a part of the atmosphere above $1.05\,R_{\odot}$ (Scudder & Karimabadi 2013). These lacunae will be important in studies that attempt to invert the heating rates of various species from such incomplete conservation laws.

In this paper the general size of the TF density is shown to be determined by a local moment-like integral over the electron velocity probability distribution function (eVDF); it is nonzero when the eVDF possesses an odd pitch angle symmetry in the plasma rest frame. The TF is closely related to other more frequently encountered eVDF moments with a similar sensitivity: the field-aligned current and heat flux.

The size of the TF depends inversely on the rate of processes that would symmetrize the eVDF. However, such scattering processes are in competition with other agents, like the underlying $E_{\|}$, that act to distort the eVDF, giving it skewness and impacting the size of both the TF and the heat flux. The TF as a net residual, depends on the results of these competitions between *symmetrization* and *deformation* of the eVDF. Microphysically the finiteness of nonzero Coulomb scattering frequency ν_{ei} scales the rate of binary momentum transfer.

If the symmetrization effects of collisions were the sole determinant of the size of the TF, one might expect that the TF would approach zero in the strongly collisional Spitzer regime, scaling inversely with *increasing* ν_{ei}. However, in this regime it is known that the symmetrization and distortion tendencies compensate, leaving a net result in the absence of $J_{\|}$ called the TF that does *not* scale with the binary rate of collisions (Braginskii 1965; Fitzpatrick 2014). The solar wind at 1 au is not like that supposed by Spitzer and is shown below to have an even more counterintuitive inverse scaling with *decreasing* collision frequency.

Below the TF's importance is demonstrated to *grow with the size of the Knudsen number*, being the largest in the high-speed solar wind traditionally characterized as the *least collisional*. The parallel electric field is shown to be an important factor in the growth of the TF, which is shown to scale directly with the size of $E_{\|}$, while scaling inversely with the local Coulomb

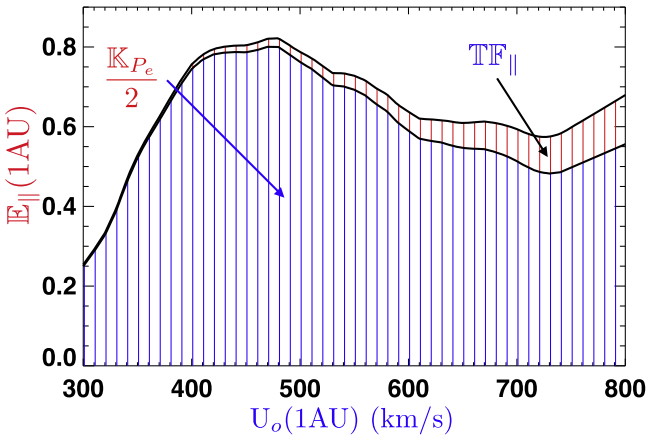

Figure 1. Estimated partition at 1 au of the dimensionless $\mathbb{E}_\parallel = E_\parallel/E_D$ as a function of bulk speed U from the measurement of terms of the GOL showing the additive (red) correction from $\mathbb{TF}$ to that from the (blue) pressure Knudsen number, $\mathbb{K}_P$.

collision frequency. From these observations the tendency to "grow" eVDF asymmetry in the finite Knudsen regime apparently overpowers the available processes that can remove it, leaving the TF an important player in any fluid-scale description of heat-conducting astrophysical plasmas.

The TF should be considered as omnipresent in astrophysical plasmas since its role scales with the importance of conduction heat flows in the plasmas; these are invariably important in astrophysical plasmas, especially those hot enough to remain fully ionized and thus proficient conductors of heat.

The moment form of a heat closure cannot be uniquely inverted to determine the TF that corresponds to it. The absence of the TF in astrophysical plasma modeling is a direct corollary of the ad hoc way that heat law closures are introduced at the moment level without an underlying eVDF predicate for their origin (Breech et al. 2009; Cranmer et al. 2009). The infinitesimal $\mathbb{K}_P$ approach of Chapman–Enskog (Chapman 1916; Enskog 1917) determines the transport modifications for the eVDF and then makes sure they produce force balance in the generalized Ohm's law, hereafter GOL (Rossi & Olbert 1970). This type of construction is a part of the kinetic transport discussions of Spitzer (1965), Braginskii (1965), Ferziger & Kaper (1972), and Balescu (1988), for infinitesimal $\mathbb{K}_P$ regimes. Because of the perturbative nature of these *forward* constructions of the TF, they are not appropriate for astrophysical fluid plasma modeling in the omnipresent finite $\mathbb{K}_P$ regime.

To address the observable profiles of electrons and ions separately, at least a two-fluid description is required and the role of the TF cannot be suppressed. Below it is shown that the TF changes the structure of the electron and ion internal energy equations, preferentially cooling the electrons and heating the ions. If the TF is unavailable, suppressed, or ignored, these redistributions of internal energy cannot occur in the modeling, although they are enabled in nature. Until this self-consistency is assured the plasma fluid equations do not make predictions worthy of quantitative comparison with observations. Conversely, observations compared with fluid modeling with inconsistent closures, yield no conclusion except that of a *hung jury* (Scudder 2019a).

The TF on electrons strengthens the equilibrium radial outward parallel electric field (for $J_\parallel = 0$) beyond that inferred from $-\nabla \cdot P_e/en_e$ alone (see Figure 1 for estimates). Thus, the $\mathrm{TF}_\parallel$ enhances the depth of the electrostatic well for electrons in the solar wind and corona, using the leading-order field-aligned components of the electron momentum equation:

$$\begin{aligned} eE_\parallel &= -\frac{\hat{\boldsymbol{b}} \cdot \nabla \cdot P_e}{n_e} + \mathrm{TF} \cdot \hat{\boldsymbol{b}} \\ \mathbb{E}_\parallel &= \tfrac{1}{2}\mathbb{K}_P + \mathbb{TF}_\parallel \\ \mathbb{E}_\parallel &\equiv \frac{E_\parallel}{E_D}, \end{aligned} \tag{2}$$

while simultaneously allowing strong heat flow skewness with $J_\parallel = 0$, since enhancing $E_\parallel$ enhances the suprathermal fractional density in the eVDF (Scudder 2019b). The second equation above proceeds from the first by scaling by eE_D, where E_D is Dreicer's electric field (Dreicer 1959, 1960) defined by

$$\begin{aligned} eE_D \equiv \frac{nm\Gamma_e}{w_e^2} &= mw_e\nu(w_e) = \frac{2kT_e}{\lambda_{\mathrm{mfp}}} \\ \Gamma_e &= \frac{\nu(w_e)w_e^3}{n}, \end{aligned} \tag{3}$$

where $\nu(w_e)$ is an electron–ion collision frequency at speed w_e (Dreicer 1959) that can be given a precise definition via Equation (9) in Dreicer (1959). The parallel electron pressure Knudsen number, $\mathbb{K}_P$, of Equation (1) arises naturally in the GOL as the ratio of the field-aligned pressure gradient force to eE_D. The dimensionless TF is defined by

$$\mathbb{TF}_\parallel \equiv \frac{\mathrm{TF}_\parallel}{eE_D}. \tag{4}$$

The existence of a heat flux TF coordination implies that there is a Coulomb scattering moderated electron heating rate ν_E^{TF} for electrons that outpaces the Coulomb energy exchanges $\nu_{E,ei}^{\mathrm{Gauss}}$ (between Gaussian ion and electron distributions) by at least the factor $m_p/(3m_e)$. Explicit incorporation of the TF effects modify the structure of the separate electron and ion internal energy equations in two ways: introducing exchanges not present in multifluid gas dynamics through second-order Stokes processes and second-order ohmic losses, discussed below in Section (7).

2. Is Electron–Ion Friction Important in the Solar Wind?

Slippage friction (usually termed Stokes friction) occurs when two fluids coupled by collisions are in relative motion, with different mean flow velocities. The neutral fluid plasma model postulates common bulk motions of ions and electrons. In this fluid treatment of the plasma there is no (first-order) Stokes friction between electrons and ions despite the presence of Coulomb interactions.

The existence of the TF is synonymous with the skewness in the eVDF that accompanies heat flow. It is a useful straw model to think of a skewed eVDF as produced by the sum of two Gaussians drifting slowly with respect to one another along the magnetic field (as indicated in Figure 2). If such an eVDF is to be a proxy for a neutral fluid moving with the flow velocity of the protons, the densities, $n_{e,j}$ and the inertial frame Gaussian flow velocities $\boldsymbol{U}_{e,j}$ will be coordinated so that

$$\begin{aligned} n_{e,1}\boldsymbol{U}_{e,1} + n_{e,2}\boldsymbol{U}_{e,2} &= (n_{e,1} + n_{e,2})\boldsymbol{U}_+ \\ n_{e,1}\Delta_{e,1} &= -n_{e,2}\Delta_{e,2}, \end{aligned} \tag{5}$$

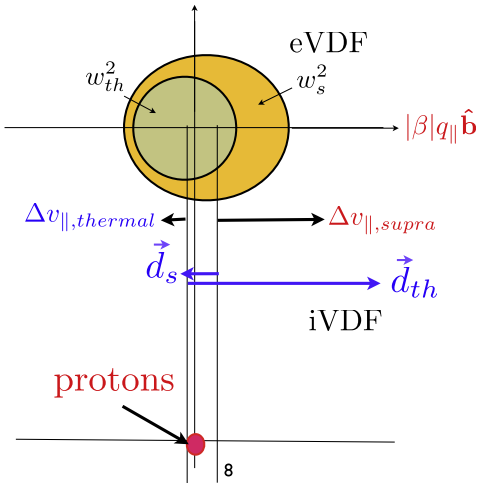

Figure 2. A conceptual diagram of the TF, where the skewness of the eVDF is modeled by two drifting isotropic Gaussians with different temperatures and densities. Such a model has been used to characterize a large body of solar wind electron data (Feldman et al. 1975).

where the electron-component, field-aligned slippages in the ion frame are given by $\Delta_{e,k} \equiv (\boldsymbol{U}_{e,k} - \boldsymbol{U}_+) \cdot \hat{\boldsymbol{b}}$. If the *component* electron partial densities, $n_{e,j}$, are different, the underlying slippage speeds $\Delta_{e,j}$ will be anti-collinear. To model zero current and finite skewness (heat flow) the rms thermal speeds of the two Gaussian components must be different (see Equation (24)); this produces a different scattering rate between thermal electrons and ions as opposed to suprathermals with ions, causing a nonzero TF parallel to $\boldsymbol{q}_{\|,e}$.

The core–halo form for the modeled solar wind spectra (Feldman et al. 1975; shown in Figure 2) is a superposition of two Gaussian distributions (green and yellow) in the upper part of the figure (thermal/core and suprathermal/halo). By observations (Feldman et al. 1975) these (core–halo) subpopulations have (higher-lower) densities and (lower-higher) rms widths in velocity space, and drift along $\hat{\boldsymbol{b}}$ (lagging-leading) the much narrower ion distribution (red dot) that determines the center of mass of the plasma.

The dissimilar electron sub-fluids are the thermal and suprathermal components with different fractional densities, and rms thermal spreads that as a tandem support the heat flow (skewness) of the electron eVDF. The skewness supported by these two components has been modeled from observations (Feldman et al. 1975) as the result of counterposed field-aligned flow speeds in the ion rest frame. Together with their different densities these drifts are consistent with representing no parallel current in the ion rest frame as shown in Figure 2.

Conceptually the TF is the net result of the two oppositely sensed Stokes drags, $\overline{\boldsymbol{d}}_s$, $\overline{\boldsymbol{d}}_{\rm th}$ (for the suprathermal (s) and thermal (th) drags) with the protons via Coulomb scattering. The net drag is always dominated by the *cooler* thermal electron "Stokes" contribution, giving the TF the same sense as $\overline{\boldsymbol{d}}_{\rm th}$ and that of $q_{\|}$. With this competition the TF is a second-order Stokes friction result. The possibility of a TF arises from the plasma's strongly speed-dependent Coulomb collision frequency and has no analog in heat-conducting neutral gas dynamics.

3. Fokker–Planck Description of Coulomb Drag

The Fokker–Planck drag between a general gyrotropic electron distribution function $f_e(\boldsymbol{v})$ and a distribution of ions with rest frame velocity $\boldsymbol{U}_i$ is discussed as a preparatory calculation for determining the TF without recourse to model-dependent expressions, as found in the Braginskii summary (Braginskii 1965). Because of the mass disparity ions are well modeled for scattering as delta functions in velocity space.

The dimensionless eVDF F_e is defined so that

$$f_e(\boldsymbol{v}, \boldsymbol{U}_e) \equiv \frac{n}{\pi^{3/2} w_e^3} F_e(\boldsymbol{v}), \tag{6}$$

where $\boldsymbol{v}$ represents the inertial frame velocities of the individual electrons. n, $\boldsymbol{U}_e$, and w_e are determined by the first three moments of the eVDF. With this approach F_e is dimensionless.

From Rosenbluth et al.'s (1957) Fokker–Planck formulation the drag on electrons caused by the ions possessing a bulk velocity $\boldsymbol{U}_+$, takes the form

$$\begin{aligned} \boldsymbol{d} &= \frac{mn\Gamma_e}{\pi^{3/2} w_e^3} \int d^3v F_e(\boldsymbol{v}) \nabla_{\boldsymbol{v}} \frac{1}{|\boldsymbol{v} - \boldsymbol{U}_+|} \\ \boldsymbol{d} &= -\frac{mn\Gamma_e}{\pi^{3/2} w_e^3} \int d^3v F_e(\boldsymbol{v}) \frac{\boldsymbol{v} - \boldsymbol{U}_i}{|\boldsymbol{v} - \boldsymbol{U}_+|^3}. \end{aligned} \tag{7}$$

Here we have introduced $\Gamma_e \equiv 4\pi (e^2/m_e)^2 \mathrm{Log}(\lambda_D/p_o)$, where $\lambda_{\rm D}$ is the Debye length and p_o is the average impact parameter for 90° scattering. Since $n\Gamma_e w_e^{-3}$ is a frequency one can easily show that Equation (7) has the units of a force. Using $\boldsymbol{g} \equiv \boldsymbol{v} - \boldsymbol{U}_+ = w_j \bar{\zeta} - \boldsymbol{U}_+$ and $d^3g = d^3v = w^3 d^3\zeta$ we obtain

$$\begin{aligned} \boldsymbol{d} &= -\frac{mn\Gamma_e}{\pi^{3/2} w_e^2} \int d^3\zeta F_e(w_e \bar{\zeta}) \frac{\hat{\zeta}}{\zeta^2} \\ \frac{\boldsymbol{d}}{eE_D(w_e)} &= -\frac{1}{\pi^{3/2}} \int d\zeta d\mu_\zeta d\phi_\zeta F_e(w_e \bar{\zeta}) \hat{\zeta} \\ \frac{d_{\|}}{eE_D(w_e)} &= -\int d\zeta \mathbb{L}(\zeta, \Delta) \\ \mathbb{L}(\zeta, \Delta) &\equiv \frac{2}{\sqrt{\pi}} \int_{-1}^{+1} d\mu_\zeta \mu_\zeta F_e(w_e \bar{\zeta}, \mu_\zeta), \end{aligned} \tag{8}$$

where the pole for $\bar{\zeta}$ is selected to be that of $q_{e,\|}\hat{\boldsymbol{b}}$ or $\hat{\boldsymbol{b}}$ with preference for the vector set by the sense of $q_{e,\|}$ if it is nonzero. With this understanding we define

$$\hat{\boldsymbol{q}}_{e,\|} \equiv \frac{q_{e\|}}{|q_{e\|}|} \hat{\boldsymbol{b}}. \tag{9}$$

The notation $\mu_\zeta = \hat{\zeta} \cdot \hat{\boldsymbol{b}}/\zeta$ has also been introduced. For future reference the definition of $\mathbb{L}$ contains its dependence on the electron's relative drift, Δ, along $\hat{\boldsymbol{q}}_{e,\|}$ as seen in the ion's rest frame.

In this way the drags considered include three classes of eVDFs: (i) those drifting with respect to $\boldsymbol{U}_+$, but possessing no heat flow in their bulk speed rest frame, $\boldsymbol{U}_e$; (ii) those not drifting with respect to the ions $\boldsymbol{U}_e = \boldsymbol{U}_+$ but possessing a heat flow; and (iii) those drifting relative to ions *and* possess heat flow in the $\boldsymbol{U}_e$ frame. Modeling of class (i) recovers Stokes friction; (ii) TF friction; and (iii) the general possibility.

The usual fluid model of a plasma pertains to class (ii). En route to developing the general form for the TF in this regime, we first demonstrate that the general analysis recovers the special case (i) considered by Dreicer of a Gaussian eVDF drifting in the ion heat frame.

If the eVDF, f_e, is defined in the ion rest frame, then clearly $\boldsymbol{g} \equiv \boldsymbol{v} - \boldsymbol{U}_+ = w_e \bar{\zeta}$. In the case (i) above, the electrons are

isotropic in their own frame, but by drifting $\Delta \equiv \boldsymbol{U}_e - \boldsymbol{U}_+$ in the ion frame $F_e(\bar{\zeta})$ will depend on the cosine, μ_ζ, of the polar angle in the ion frame. The drifting property of f_e will have a nonzero projection along $P_1(\mu)$ and a nonzero drag and $\mathbb{L}(\Delta) \neq 0$. This leads to Stokes (first -order) drag studied by Dreicer (1959).

Alternately, if the eVDF considered does not drift with respect to the ions, then μ_ζ reverts to the traditional electron pitch angle in the $\boldsymbol{U}_e = \boldsymbol{U}_+$ rest frame, where the last integral in Equation (8) can *still* be nonzero if the pitch angle distribution supports a *skewness* that signals supporting a heat flow. If it does, the eVDF projection along $P_1(\mu_\zeta)$ can remain nonzero, and there will be a TF friction. In this case as shown in Figure 2 the net result involves the residual of the competition of two opposing drags $\boldsymbol{d}_j$; each of these drags would be a first-order Stokes drag; the competed answer is the TF, the residual of second-order Stokes effects.

3.1. Drag Properties for General $f_e(\boldsymbol{v})$

Specializing Equation (8) to an $f_e(\boldsymbol{v})$ that is the entire electron population, certain general conclusions can be drawn. To clarify the conditions on integrals for the entire eVDF, this complete eVDF will be indicated by $f_{e,\Sigma}(\boldsymbol{v}, \Delta = 0)$ using the Σ subscript to imply that it is the entire eVDF and that it is presumed at rest in the ion frame, $\Delta = 0$.

Upon inspection $\mathbb{L}_\Sigma$ is the projection of f_Σ along the Legendre polynomial $P_1(\mu_\zeta) = P_1(\mu)$. The net size of the drag depends on the subsequent nonzero value of the speed integral over ζ.

Since the net drag for f_Σ is $\boldsymbol{d}_\parallel$, a special case of three-related (moment) integrals of the eVDF given by the common form:

$$\mathcal{G}_\Sigma(r) \equiv \frac{2nw_e^r}{\sqrt{\pi}} \int_0^\infty \left[\int_{-1}^{+1} d\mu F_{e,\Sigma}(\boldsymbol{w}_e \bar{\zeta}) P_1(\mu) \right] \zeta^{2+r} d\zeta, \quad (10)$$

there is new leverage about the TF made possible by a brief detour into the three cases:

$$\begin{aligned} m\Gamma_e \mathcal{G}_\Sigma(-2) &\equiv -d_\parallel = -eE_D \mathbb{TF}_\parallel \\ e\mathcal{G}_\Sigma(1) &\equiv J_\parallel \\ m\mathcal{G}_\Sigma(3) &\equiv 2q_\parallel, \end{aligned} \quad (11)$$

where $J_\parallel$ and $q_\parallel$ are the parallel electrical current and heat flux, respectively. With a common μ integral, the $\mathcal{G}(r)$ integrands differ only by their weighting powers, $2 + r$, of nonnegative speed. For the fluid plasma model with $\boldsymbol{U}_e = \boldsymbol{U}_i$ and $\mathcal{G}(1) = 0$, $\mathbb{L}_\Sigma(\zeta)$ must have regions of opposite signs. Since the nonnegative ζ weights increase with the size of r, the weighted areas of different signs in $\mathcal{G}(n)$ must grow monotonically when proceeding from $r = \{-2, 0, 3\}$, making $\mathcal{G}(-2) < 0 < \mathcal{G}(3)$ and thus of opposite signs.

This argument, together with the definitions in Equation (11), proves the general theorem: if $\mathcal{G}(1) = 0$ the sign of $\mathbb{TF}_\parallel$ and $q_{e,\parallel}$ must be the same, with the general form for $\mathbb{TF}$ given by

$$\mathbb{TF}_\parallel \equiv -\int d\zeta \mathbb{L}_\Sigma(\zeta, \Delta = 0) \hat{\boldsymbol{q}}_{e,\parallel} \quad (12)$$

$$\mathbb{L}_\Sigma(\zeta, \Delta = 0) \equiv \frac{2}{\sqrt{\pi}} \int d\mu \mu F_{e,\Sigma}(\zeta, \mu, \Delta = 0) \quad (13)$$

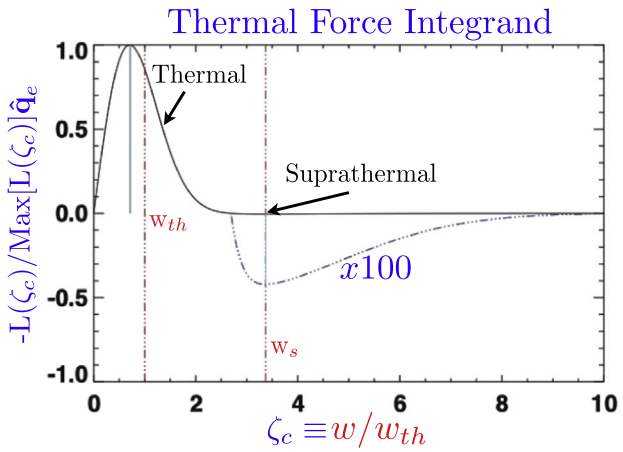

Figure 3. Speed integrand for the TF using the two-component core–halo model. Note the suprathermal contribution is slightly negative and seen better with 100× magnification.

$$F_{e,\Sigma} \equiv \frac{\pi^{3/2} w_e^3}{n_e} f_{e,\Sigma}\left(\bar{\zeta} = \frac{\boldsymbol{v} - \boldsymbol{U}_+}{w_e}\right). \quad (14)$$

Figure 3 illustrates the integrand L_Σ for the TF determination using the core–halo eVDF, assuming zero current and typical 1 au solar wind parameters. This integrand represents the appropriate sum of contributions for the separate subcomponents. As the thermal form has a specific normalization in terms of the properties of f_Σ, L_Σ is slightly different than the sum of contributions from each component separately.

The oppositely signed contributions of the core and halo components are made clearer by the 100× magnification of the negative suprathermal contribution to the integrand. For counterdrifting Gaussian components (required for $J_\parallel = 0$) the maximum moduli of contributions to the integrand are at slightly less that the rms speed of each subcomponent. The null of the integrand lies between these values as implied by where the magnified negative profile clearly emerges from below 0.

Three factors visibly weaken the amplitude of the integrand at suprathermal speeds: their (i) small fractional density; (ii) higher rms speed that spreads the eVDF out more in velocity space than the thermals at unit density, and (iii) the differentially weakened scattering rate of the suprathermals in the speed-dependent Coulomb scattering off the ions. The net TF is a vestige in heat-conducting plasmas of the strong speed dependence of the Coulomb scattering cross section, causing $\mathrm{TF}_\parallel$ to be dominated by the cooler electron subpopulation (see Figure 3).

3.2. Dreicer Stokes Drag Recovery for Gaussian

However, if $f_{e,j}$ is but a part of the complete eVDF, then *its* apparent drift speed Δ_j in the ion frame may not vanish, provided it is counterposed by other components that bring the entire eVDF to move with the ion bulk speed. If, as observed in the solar wind (e.g., Feldman et al. 1975), the different electron subcomponents drift in the ion frame along the magnetic field direction, each component's velocity space described in the ion rest frame remains cylindrically symmetric about $\hat{\boldsymbol{q}}_e$. Thus, each $\boldsymbol{d}_j$ determines the drag felt by that electron subcomponent. The convection of that component in this frame will be that caused by the relative motion between the j'th electron species and the ions. We denote for further use below the thermal mach

number of the j'ths component relative field-aligned drift mach number as $\mathcal{M}_j \equiv \Delta_j/w_{ej}$.

The drag realized by a *single-drifting Gaussian* subcomponent should recover the (first-order) Stokes drag studied by Dreicer (1959); in so doing Equation (12) is supported as the appropriate TF generalization for an arbitrary gyrotropic f_e. The structure of the angular average $\mathbb{L}_i$ for a drifting Gaussian with thermal mach number $\mathcal{M}_i$ is of considerable interest in the physics and implications of the TF. It takes the form

$$\begin{aligned} L_i(\zeta_i, \mathcal{M}_i) &= \frac{2}{\sqrt{\pi}} e^{-(\zeta_i^2+\mathcal{M}_i^2)} \int_1^{-1} e^{\eta_i x} x dx \\ &= \frac{4e^{-(\zeta_i^2+\mathcal{M}_i^2)}}{\sqrt{\pi}\,\eta_i^2}[\sinh\eta_i - \eta_i\cosh\eta_i] \\ \eta_i &\equiv 2\mathcal{M}_i\zeta_i. \end{aligned} \tag{15}$$

For a thermal Gaussian component $f_{e,c}$ of density fraction $(1-\delta)$, thermal speed w_c, drifting with speed Δ_c, and thermal mach number $\mathcal{M}_c \equiv \Delta_c/w_c$, putting the integral of Equation (15) into Equation (8) yields

$$\frac{\boldsymbol{d}_c^{\text{Gaussian}}}{eE_D(w_e)} \equiv -\left[\frac{(1-\delta)w_e^2}{w_c^2}\right]\Psi_D(\mathcal{M}_c)\hat{\boldsymbol{q}}_e, \tag{16}$$

where the [...] specialization of the collision frequency to a w_c thermal spread and a component fractional density of $(1-\delta)$ are required, and facilitated by Equation (20) below. Dreicer's antisymmetric drag function (Dreicer 1959), Ψ_D, occurs naturally in this expression, and is defined and approximated by

$$\begin{aligned} \Psi_D(x) &\equiv \frac{\text{Erf}x}{x^2} - \frac{2e^{-x^2}}{\sqrt{\pi}x} = -\Psi_D(-x) \\ \Psi_D(x) &\simeq \frac{4x}{\sqrt{3\pi}}\left[1 - \frac{3x^2}{5} + \frac{3x^4}{14} - \frac{x^6}{18} + \frac{x^8}{88} + O(x^{10})\right]. \end{aligned} \tag{17}$$

It may seen that Equation (16) above correctly reduces to Dreicer's when (the second sparser component has no density) $\delta = 0$; when the rms speed for all electrons is that of the remaining component: $w_c = w_e$; when the mach number of the thermals is identified as that of the whole: $\mathcal{M}_c = \mathcal{M}_\Sigma$, and which implies that $\mathcal{M}_\Sigma \equiv \hat{\boldsymbol{b}} \cdot (\boldsymbol{U}_e - \boldsymbol{U}_+)/w_e$.

The form of $\Psi_D(X)$ is indicated by the black curve in Figure 4; parallel to the convention of Stokes friction, Dreicer's electron drag force is $F = -eE_D\Psi_D(X)$, opposing the sign of the drift, X. $\Psi_D(X)$ has a restricted linear regime (contrast with red dashed line) when $|X| \ll 1$. Note that typically reported core and halo drifts in the solar wind are well *below* the maximum frictions available when $|X| = 1$, indicated by orange-dotted vertical lines. Assuming an outward magnetic sector in solar wind modeling the core mach number typically is near $X_c = O(-.03)$ and halo mach numbers centered near $X_h = 0(+0.57)$; for these regimes a slightly different linear approximation in the cyan regime for the core, and a slightly different linear approximation for the larger orange regime suitable for halo values indicated by red dashed and solid blue lines through the origin have slopes of 1.0 and 0.720, respectively. These values occur in the approximate expressions in Equations (21) and (26) below. The best precision of

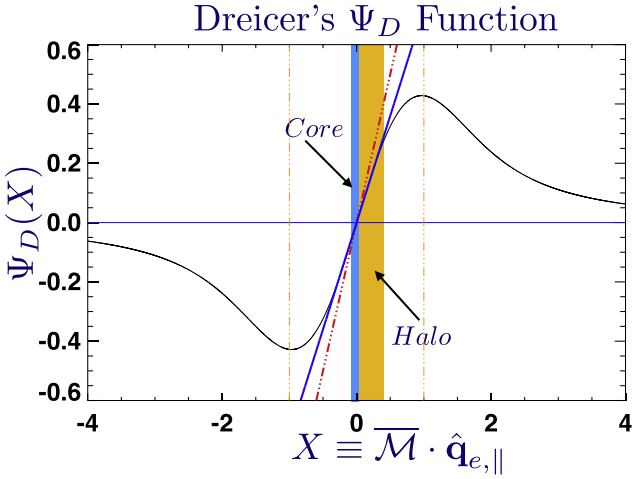

Figure 4. Variation (black) of *minus* the dimensionless Coulomb drag, Ψ, for a Gaussian electron distribution drifting with a thermal mach speed $X = \overline{\mathcal{M}} \cdot q_{e,\|}\hat{\boldsymbol{b}}$. Established by Dreicer, this convention describes the drag on fluid electrons as $-|e|E_D\Psi_D(X)$, so that the drag on electrons moving with $X < 0$ is proportional to $-\Psi_D(X < 0)$. This historical convention reproduces standard Stokes-like behavior at low drift mach numbers with the drag force opposing the sense of relative motion. The colored regions denote typical core and halo drift mach numbers for solar wind conditions near 1 au (Salem & Pulupa 2019).

the overall drag comes from using the full transcendental form of Ψ.

3.3. $\mathbb{TF}^{\text{C-H}}$ = *Net Drag for Core–Halo Gaussian eVDFs*

The superposed (core–halo) model of two Gaussian components has been used to characterize observed eVDFs in the solar wind for nearly 50 yr (Montgomery et al. 1968; Feldman et al. 1975). Equation (16) will now be specialized for two counterposed Gaussian components with unequal densities and thermal spreads and zero current to demonstrate its implications for the size of $\mathbb{TF}$ in the solar wind at 1 au.

For simplicity we consider only two electron subcomponents with counterposed drifts satisfying the zero current condition:

$$n_+[(1-\delta)\Delta_c + \delta\Delta_h] = 0 \quad \delta = n_h/n_+, \tag{18}$$

where c stands for core, h for halo, and "+" stands for the ions. The sum of drag contributions from the two subcomponents takes the form:

$$\mathbb{TF}^{\text{C-H}} = -\frac{w_e^2}{w_c^2}[(1-\delta)\Psi_D(\mathcal{M}_c) + \delta\tau^2\Psi_D(\mathcal{M}_h)]\hat{\boldsymbol{q}}_e, \tag{19}$$

where $\tau \equiv w_c/w_h$ and the needed thermal speed ratio is given by

$$\frac{w_e^2}{w_c^2} = 1 + \delta(\tau^{-2} - 1) + 2\mathcal{M}_c^2\frac{1-\delta}{3\delta}. \tag{20}$$

In Equation (20) the numerically small kinetic energy $(\mathcal{M}_c^2)$ associated with the drifting of the core and halo in the ion frame is a tiny part of the overall temperature moment for the composite distribution function; it is included here to get an accurate estimate of the moment dispersion w_e of the composite parent f_Σ.

Using Equation (19), where both the core and halo with $\mathcal{M}_i \ll 1$, and Figure 4 to motivate slightly different linear

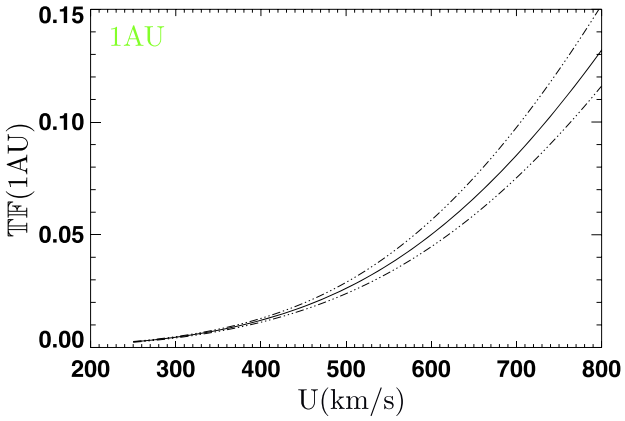

Figure 5. Estimated size of $\mathbb{TF}_{\|}$ as function of bulk speed at 1 au based on long-term variations of core–halo shape parameters (Salem & Pulupa 2019). Significance of the suggested size of $\mathbb{TF}$ can be appreciated, as this becomes nearly a 25% correction to $\mathbb{K}_P$ in the generalized Ohm's law at the higher bulk speeds (see red cross hatching; Figure 1).

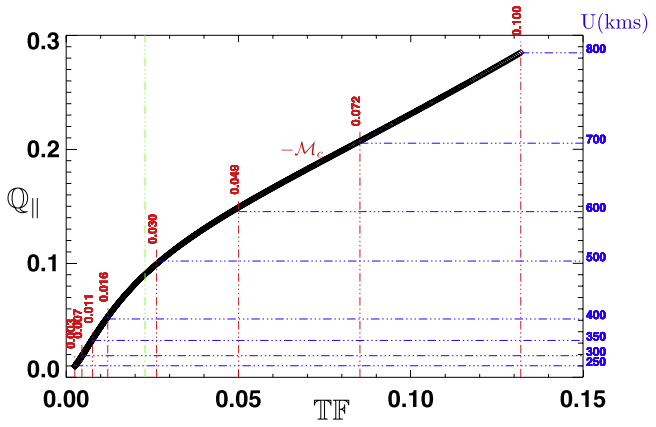

Figure 6. Demonstration that the dimensionless heat flux $\mathbb{Q}_{\|}$ and $\mathbb{TF}$ have the same sense, are 1–1 using the core–halo model 1 au parameters as a function of U summarized by Salem & Pulupa (2019).

slopes, this expression is approximately given by

$$\mathbb{TF}_{\|} \simeq -\frac{4w_e^2(1-\delta)\mathcal{M}_c}{3\sqrt{\pi}w_c^2}(1-0.720\tau^3)\hat{\boldsymbol{q}}_{e,\|}. \tag{21}$$

Equation (21) shows that $\mathbb{TF}_{\|}$ grows in magnitude with the core's thermal drift mach number. Since it is known that the core drift is enhanced in fast winds at 1 au (Pulupa et al. 2014), and the solar wind electron temperature is reduced with increasing speed (Feldman et al. (1975)), and $d\tau/dU < 0$ the TF magnitude by this estimate is expected to be larger in fast solar wind at 1 au than in slow winds.

4. 1 au Thermal Force Properties

4.1. Size

To get a further idea of the size and bulk speed dependence of the *ignored* $\mathbb{TF}_{\|}$ at 1 au we use the core–halo model and the well-known coordination of its nonthermal shape parameters with bulk speed (see summaries of Salem & Pulupa 2019) to suggest initial estimates of $\mathbb{TF}_{\|}$'s strong variation with bulk speed in Figure 5. The dimensionless TF rises steadily with solar wind speed, achieving maximum values of $\mathbb{TF}_{\|} \leqslant 0.15$. This trend is unexpected since traditionally high wind speed states are thought to be more collisionless; since Coulomb collisions are involved in the understanding of the TF, naive arguments would argue that its size would decrease with wind speed regimes where the Coulomb collision frequency was reduced.

4.2. Scaling $\mathbb{TF}$, TF with $\nu_{\rm ei}$, $\mathbb{E}_{\|}$

In the previous section the $\mathbb{TF}_{\|}$ is shown to be a sizeable term in the $\mathrm{GOL}_{\|}$ at 1 au in the high-speed wind, in what many have modeled as the "collisionless" solar wind modeled with the Vlasov equation (the collisionless Boltzmann equation). The TF relies on the existence of Coulomb collisions (Braginskii 1965; Fitzpatrick 2014); although such collisions are always present, it is incorrect to suggest that the TF importance scales just with the *frequency of the collisions*. In competition with collisions the size of the TF is *also* driven by those factors that control the skewness of the eVDF. The strong correlation of $\mathbb{TF}$ and $\mathbb{Q}$ shown in Figure 6 reflects this fact, since $\mathbb{Q}$ measures the

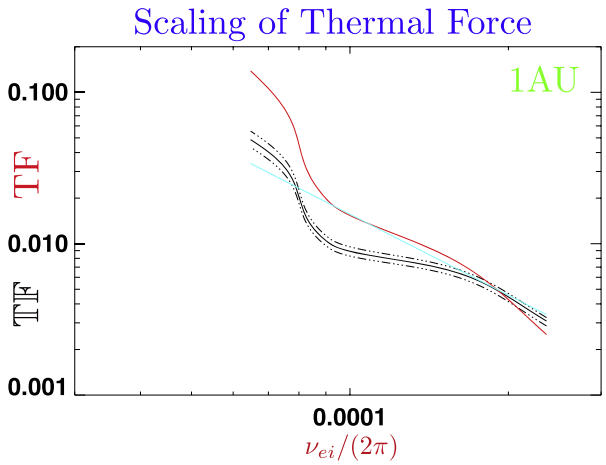

Figure 7. *Scaled* $\mathbb{TF}$ (black), *unscaled* TF (red) evaluated using core–halo model and observations (Salem & Pulupa 2019), contrasted with local collision frequency from observations. Contrary to formal ordering suggestions $\mathbb{TF}_{\|}$ is observed to be anticorrelated with collision frequency.

geometrical skewness of the eVDF and is relatively divorced from the size of the heat flow set by the number density and mean thermal energy. In a neutral gas skew deformation is the complement of fewer and fewer collisions that can isotropize the eVDF indexed by the dimensionless heat flux $\mathbb{Q} = q_{\|}/q_{\rm sat}$, where $q_{\rm sat} = 3nkT_e w_e$. However, the strong role of $E_{\|}$ in the finite Knudsen regime of the solar wind plasma permits other ways for the skewness of the eVDF to be sustained.

To be careful the dimensionless $\mathbb{TF}_{\|}$ has been mapped into its dimensional variant, $\mathrm{TF}_{\|}$

$$\mathrm{TF}_{\|}(U) \equiv eE_D(U)\mathbb{TF}_{\|}(U), \tag{22}$$

for use in Figure 7, where it is plotted versus the Coulomb collision frequency, $\nu_{ei}(U)$. Consistent with the impression from $\mathbb{TF}_{\|}$ the dimensional $\mathrm{TF}_{\|}$ is anticorrelated with ν_{ei}, despite the possibility that the variation of the scaling $eE_{\rm D}(U)$ could have changed the dimensionless trend. The observed general inverse scaling of $\mathrm{TF}_{\|}$ and ν_{ep} shows the symmetrizing role of enhanced collisions is involved in reducing the size of the TF. It is when this scaling is taken to infinite ν_{ep} regime that one incorrectly suggests that $\mathrm{TF}_{\|} \to 0$. Rather, as shown by Spitzer

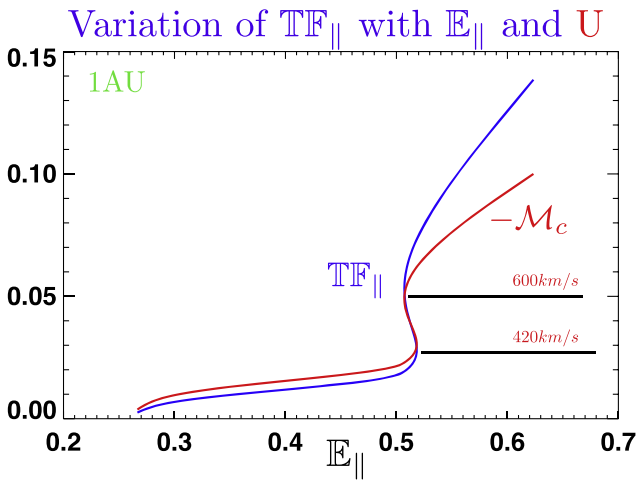

Figure 8. *Empirical* variation of $\mathbb{TF}_{\|}$ (blue) and $-\mathcal{M}_c$ (red) vs. $\mathbb{E}_{\|}$, showing a strong positive correlation, including noticeable and strong coordinated change when conditions near $\mathbb{E}_{\|} \simeq 0.5$.

and Braginskii the TF approaches an assumed infinitesimal value in their perturbative regime that is independent of ν_{ep}.

When collisional symmetrization agents of the $\mathrm{TF}_{\|}$ are weakened, the TF may strengthen, provided its driving sources remain; when collisions are stronger the $\mathrm{TF}_{\|}$ gets smaller, but may not be wiped out completely, depending on the variations of the drivers with collisional rate. In this sense the observed signatures of the TF are consistent with the symmetrizing role of collisions; however, the other determinant of its size is the persistence of skewness and omnipresence of inhomogeneity as collisions increase. To maintain quasi-neutrality, astrophysical plasmas require an $E_{\|}$ that differentially feed skewness (Scudder 2019b) that is indexed from the moments by the dimensionless heat flux $\mathbb{Q}$. This linkage is part of the deep inter-relationship between the heat flux and the TF summarized below in Equation (28) and discussed in relation to Figure 6 below.

As developed elsewhere (Scudder 2019b) this electric field causes a bifurcation of the eVDF, while driving the thermal part of velocity space in a Drude-like fashion to lag the ions. The inevitable return currents among the complementary part enhances the suprathermal deformation toward the heliopause. This *stretching* of the eVDF is controlled by $\mathbb{E}_{\|}$ that is more pronounced in the high-speed wind regimes where collision frequency goes down. Both reduced collision frequency and enhanced $\mathbb{E}_{\|}$ allow and cause the eVDF to become more skewed. Even as Coulomb collision rates go down, there is no deterioration of the speed dependence of those collisions that remain, and its is this variation of collision rate with particle speed that permits the TF to survive.

Dramatic evidence of this type of behavior is seen in Figure 8, where $\mathbb{TF}$ and $-\mathcal{M}_c$ are plotted versus $\mathbb{E}_{\|}$, showing both signatures are strongly organized by the dimensionless electric field. Of particular interest is the strong change in TF and mach number drift as $\mathbb{E}_{\|}$ approaches the vicinity of 0.5, a regime of considerable interest in runaway theory. Unlike laboratory runaway conditions that occur beyond $\mathbb{E}_{\|} = 0.43$, astrophysical plasma can be in force balance without runaway at higher $\mathbb{E}_{\|}$ values, since the TF allowed by heat flux invariably raises the point where $J_{\|} = 0$ states are in equilibrium. At the same time the occurrence of heat flow that enables the TF is a partial remedy not considered when driving a laboratory beyond its maximal friction regime. The return currents that attend the flow of heat tend to symmetrize the eVDF more nearly than the driven beam considered by Dreicer. This figure clearly shows that $\mathbb{TF}_{\|}$ is strongly organized by $\mathbb{E}_{\|}$. Since these quantities differ by the same factor from their unscaled versions, this figure also implies that the unscaled TF, $\mathrm{TF}_{\|}$, is also controlled by $E_{\|}$. It should be recalled that the size of $\mathbb{E}_{\|}$ reflects the plasma peculiar requirements to be quasi-neutral.

4.3. Term in $\mathrm{GOL}_{\|}$

The dimensionless TF is one of the three dominant terms in the parallel GOL, $\mathrm{GOL}_{\|}$. These terms are the parallel electric field, the electron pressure divergence, and the TF, which are not explicitly proportional to the electron mass. In the absence of current flow and when normalized by Dreicer's electric field, the $\mathrm{GOL}_{\|}$ takes the form

$$\mathbb{E}_{\|} = \frac{\mathbb{K}_P}{2} + \mathbb{TF}_{\|} + O(I), \tag{23}$$

where $\mathcal{I} = \mathcal{E}/(2 + \mathcal{E} + |\alpha_{Te}|)M_e^2\mathbb{K}_P$, $\mathcal{M}_e$ is the *electron* thermal mach number, $\mathcal{M}_e = |U_e|/w_e$, $\alpha_{T_e} = |d\ln T_e/d\ln r|$, and $\mathcal{E} = |d\ln U/d\ln r|$ is the very weak exponent of the local solar wind speed's increase. The estimated TF (red shading in Figure 1) makes significant corrections to the dominant contribution to $\mathrm{GOL}_{\|}$ made by $\mathbb{K}_P$, especially as the solar wind speed increases above 400 km s^{-1}. These "measurements" of the nanovolt/m $E_{\|}$ have significant corrections from the TF term and negligible corrections from inertial accelerations.

The Lemaire–Scherer electric field (Lemaire & Scherer 1973) is exospheric theory's version of the parallel electric field, while the TF contribution of Spitzer (1965), Braginskii (1965), Fitzpatrick (2014), and this paper pertain to the size of the last term (right-hand side (rhs)) in $\mathrm{GOL}_{\|}$. Thus, the TF is but a part of, and does not contain the Lemaire–Scherer field in its entirety.

The Lemaire–Scherer field is the required $E_{\|}$ in the zero collision picture to produce quasi-neutrality and zero current; it plays precisely the same physical role as $E_{\|}$ of the $\mathrm{GOL}_{\|}$. The collisionless approach determines $E_{\|}$ directly within its *Vlasov closure*. The $\mathrm{GOL}_{\|}$ estimates $E_{\|}$ indirectly from a *two-fluid collisional closure*. Since such weak $E_{\|}$ cannot be directly measured, its size must be estimated, as shown in Figure 1, as the sum of all the parts of the rhs of the GOL that *are now* measurable. One of these parts is the TF reported in the present paper, and the other is the pressure Knudsen number that can be inferred from measured radial gradients.

4.4. Impact on Size of $\mathbb{E}_{\|}$

As shown above $\mathbb{TF} < 0.15$. Previous estimates (Scudder 1996, 2019c; Issautier et al. 1998) of $\mathbb{E}_{\|}$ from the pressure divergence or Knudsen number term in Equation (23) yield estimates that are generally larger in the high-speed solar wind; there $\mathbb{TF}$ provides as much as a 30% enhancement to $\mathbb{E}_{\|}$. Because the radial sense of $\mathbb{TF}_r$ is aligned with that of the heat flow, it is invariably radially outward; thus, the TF adds to the average contribution to $E_{\|}$ produced by $\mathbb{K}_P$, which is always positive in the radial direction when the pressure profile decreases with radius.

These modeled estimates for $\mathbb{K}_P(U)$ implied by Figure 1 and those of Figure 5 above for $\mathbb{TF}(U)$ give a first post Knudsen number picture in Figure 1 of the variation of $\mathbb{E}_{\|}(U)$. The composite preliminary picture shows, as expected, that (i) $\mathbb{E}_{\|}$ is a generally rising function of U, consistent with its theoretical role in levitating the ions out of their gravitational trap. (ii) It is uniformly *non-perturbative* in the sense of being $\mathbb{E}_{\|}(U) = O(1)$, as reported earlier (Scudder 1996). More precise bulk speed patterns will be possible when the TF contributions are determined directly from observed, rather than modeled eVDFs.

In addition, new implications are that (iii) this is the domain where the $\mathbb{TF}$ is increasingly important, despite its size being determined by sparse, but nonvanishing, Coulomb collisions. (iv) Here the $\mathbb{TF}$ *adds* to the already positive value of $\mathbb{K}_{P,\|}$, enhancing the size of $\mathbb{E}_{\|}$ in ways not being presently considered by fluid models for astrophysical plasmas. (v) The presence of the $\mathbb{TF}$ implies a significant energy heating of the electrons thousands of times more vigorous than the energy exchange rate estimated between Gaussian electron–proton distributions as two Gaussians with different temperatures. (vi) The strength of the $\mathbb{TF}$ testifies to an important role for Coulomb collisions, since the dominant part of the force occurs for electrons with low speeds compared to the rms thermal speed, where the collisional time is orders of magnitude shorter than the Coulomb scattering rate for the rms electron. The likelihood that *collisionless* instabilities resonant with the shifted thermal electrons and their stand-alone wave-particle regulation are meaningful by themselves is brought into question. A more nuanced picture of the plasma is required to predict the potential role of Vlasov-modeled resonant instabilities driven by the small mach number drifts of the core (Forslund 1970; Gary et al. 1975).

5. $\mathbb{TF}$ Impact on Energy Equation

At first the connection between the TF (a rate of momentum) and the heat flow (a rate of energy flow) seems a bit forced; the $\mathrm{TF}_{\|}$ relationship to $E_{\|}$ is clear from the momentum equation and the $\mathrm{GOL}_{\|}$, Equation (23). The purpose of this section is to clarify the role of the TF in the two-fluid energy equation, its close connection to the heat flow, and its substantial role in constraining a fluid plasma as two fluids with separate internal energy equations.

Starting from the empirical evaluation of the TF and heat flux in the framework of the core–halo model, it is possible to exhibit the strong 1–1 correspondence and alignment of the heat flux and the TF well into the finite Knudsen regime, where Spitzer (1965) and Braginskii (1965) provide no guidance.

This is followed by careful reconstruction of the two-fluid equations for the *fluid* plasma, (neglecting Stokes first-order friction: $J_{\|} = 0$), retaining second-order Stokes friction, (TF), and looking for its *footprint* in the conservation laws of the internal energy equations. Using observations the incidence of strong signatures in the radial rate equations for the internal energy of the electrons and ions are estimated for the solar wind at 1 au. The TF is shown to facilitate sizable exchanges of available internal energy by augmenting electron cooling in the plasma, leaving more internal energy available for the protons —assuming no new supply of internal energy is available.

This same bookkeeping exercise suggests that there is also a new, second-order electron ohmic heating caused by the proton drag on each subcomponent of the heat-conducting eVDF. This energy source, S_e, for the electrons is a sink for the ions, and its size is shown to be O(1000) times bigger than the pro forma energy exchange rates involving $T_e - T_i$ differences usually included (but found to be ineffective) in two-fluid models for the solar wind (Hartle & Sturrock 1968; Breech et al. 2009; Cranmer et al. 2009; Chandran et al. 2011). Overall, the TF rate of electron (ion) cooling (heating) is enhanced by the consideration of the TF, rather than neglecting it. The spirit of the "cooling" and "heating" concerns the increment to $\nabla \cdot q_j$ made by the process. Cooling makes the negative divergence more negative, while heating makes the local negative divergence *less* negative.

Conversely, given a closure and a specified $\nabla \cdot \boldsymbol{q}_j$ the explained role of the TF clarifies that sizable channels exist for exchanging heat made available by the j'th species to modify the temperature profiles of the ith species—that are presently not included in the most recent two-fluid plasma modeling of the solar corona.

6. $\mathbb{TF}$, $\mathbb{Q}$ Correlations

6.1. Core–Halo Heat Flux, $\mathrm{q}_{\|}$

The *heat flux* using the core–halo model is given by

$$q_{\|}^{\mathrm{C-H}} = -\frac{5}{2}\mathcal{M}_c n(1-\delta)kT_c w_c(\tau^{-2}-1) \times\left(1+\frac{2\mathcal{M}_c^2(1-2\delta)\tau^2}{5\delta^2(1-\tau^2)}\right). \tag{24}$$

Scaling $q_{\|}$ via the saturated heat flux, $q_{\mathrm{sat}} \equiv 3n_e kT_e w_e$, yields the dimensionless heat flux, $\mathbb{Q}_{\|} \equiv \dfrac{q_{\|}}{q_{\mathrm{sat}}}$, given by

$$\mathbb{Q}_{\|}^{\mathrm{C-H}}\hat{\boldsymbol{b}} = -\frac{5}{6}\mathcal{M}_c\frac{w_c^5}{w_e^5}(1-\delta)(\tau^{-2}-1) \times\left(1+\frac{2\mathcal{M}_c^2(1-2\delta)\tau^2}{5\delta^2(1-\tau^2)}\right), \tag{25}$$

where $m_e w_e^2 \equiv 2kT_e$. The *approximate* relationships for the TF and the dimensionless heat flux in Equations (21) and (25), algebraically motivate that the $\mathbb{Q}_{\|}$ and $\mathbb{TF}$ are proportional at small $\mathcal{M}_c$ values. As motivated elsewhere (Scudder 2019b) the size of $-\mathcal{M}_c$ scales with the strength of $E_{\|}$, hinting that the $\mathbb{TF}$ and $\mathbb{Q}$ will be well organized by $\mathbb{E}_{\|}$.

6.2. Functional Dependence: $\mathbb{Q}$, $\mathbb{TF}$

In the small Knudsen number regime where $E_{\|}$ and the heat flow is perturbative, Equations (21) and (25) determine the expected leading-order linear correlation between dimensionless heat flow and TF, viz.,

$$\mathbb{Q}_{\|} = \mathbb{TF}_{\|}\frac{5\sqrt{\pi}(1-\tau^2)w_c^3}{16(\tau^2-0.720\tau^5)w_e^3}(1+G(\mathbb{TF}_{\|}^2)), \tag{26}$$

where

$$G(\mathbb{TF}^2) = \frac{9\pi(1-2\delta)\tau^2 w_c^4\mathbb{TF}^2}{40(1-\delta)^2\delta^2(1-\tau^2)(1-.720\tau^3)^2 w_e^4}. \tag{27}$$

As $\mathbb{TF}$ goes to zero, or equivalently is ignored, the heat flux also disappears. Equation (26) is rigorous in this conclusion that these two effects are either (i) both not zero and parallel or (ii) are both zero.

Developing a solution for an astrophysical fluid plasma with a heat closure without its attendant TF is inconsistent. This can

be seen in Equation (11), since the existence of $q_{\|}$ implies $\mathbb{L}$ is nontrivial, which implies the TF will also be.

6.3. More Precise $\mathbb{Q}_{\|} = \mathcal{F}(\mathbb{TF})$

The unapproximated expressions for $\mathbb{Q}$ and $\mathbb{TF}$ Equations (19) and (25), based on observed (Salem & Pulupa 2019) statistically correlated 1 au variations of $\delta(U)$, $\tau(U)$, $\mathcal{M}_c(U)$ demonstrate in Figure 6 the overall 1–1 correlation between $\mathbb{Q}$ and $\mathbb{TF}$. Grids for the variation (in the 1 au data) of the core mach number drift, $-\mathcal{M}_c$ (red), and the variation of the solar wind speed, U (blue), are overlaid on this figure to produce context.

The realized functional relationship shows generally that (i) these two variables are related in a 1–1 manner; and (ii) that the TF and heat flux are aligned (as generally argued above); while documenting (iii) *typical* extremes of these variables and (iv) their underlying wind context. Higher $\mathbb{Q}_{\|}$ and $\mathbb{TF}$ occur in the fast wind. This correlation shows that $\mathbb{TF}$ is sensitive to the skewness, or deformed shape, of the eVDF inventoried by $\mathbb{Q}$.

This trend for 1 au observations has been approximated by *one* branch of a hyperbola

$$\mathbb{Q}_{\|} \simeq 3.13962\mathbb{TF} + 0.0581922 - 0.5(0.0135453 - 0.781819\mathbb{TF} + 13.0007\mathbb{TF}^2)^{1/2}. \quad (28)$$

An alternate form for this relationship with $\mathbb{Q}_{\|}$ as the independent variable is

$$\mathbb{TF} \simeq 0.475194\mathbb{Q}_{\|} - 0.041378 + 0.075677 \times [0.298959 - 3.86409\mathbb{Q}_{\|} + 13.0007\mathbb{Q}_{\|}^2]^{1/2}. \quad (29)$$

7. $\mathbb{TF}$: Internal Energy Equations

In this section the role of the TF in the plasma fluid energy equations is outlined and the consequences of its remainder being undefined are discussed for the internal energy equations of electrons and ions.

7.1. $\mathbb{TF}$ *Restructures* Both

The general j'th species energy equation (including all sources to it, S_{ji}) is given by Meyer-Vernet (2007):

$$\nabla \cdot \left(n\boldsymbol{U}\left[\frac{1}{2}m_j U^2 + \frac{5}{2}kT_j + Z_j e\Phi_E + m_j\Phi_G\right] + \boldsymbol{q}_j\right) = \mathrm{S}_{ji}$$
$$nU_r r^2 \frac{d}{dr}\left(\frac{1}{2}m_j U_r^2 + \frac{5}{2}kT_j + Z_j e\Phi_E + m_j\Phi_G\right) = -\frac{d}{dr}(r^2 q_{j,r}) + S_{ji}r^2, \quad (30)$$

where $Z_e = -1$, $Z_p = +1$, Φ_E and Φ_G are the electrical and gravitational potentials, respectively. The second form assumes a spherically symmetric description of the wind.

The full electron momentum equation given by

$$mU_r\frac{dU_r}{dr} + \frac{1}{n}\frac{d(nk_B T_e)}{dr} = e\frac{d\Phi_E}{dr} + \mathrm{TF}_r + m\frac{d\Phi_G}{dr} \quad (31)$$

incorporates the TF drag, TF_r, between the electrons and ions. Note the assumed absence of electron–ion first-order Stokes friction within this plasma two-fluid model, but that the $\mathrm{TF}_r > 0$ remains as a residual frictional coupling, opposing the sunward directed electric force on the electrons. It is in this sense that the TF is a second-order Stokes friction, not because it is necessarily small, but precisely because the first-order Stokes friction vanishes by postulating a fluid plasma. Because the heat flow asymmetry is so large, TF_r can represent a significant source of collisional coupling between the species, especially as the solar wind speed increases *even though there is no parallel current involved*. One measure of the strength of this coupling has already been shown in Figure 1, where the $\mathbb{TF}_{\|}$ is shown to rise from 0.1% → 30% of the size of $E_{\|}$ between 400 and 800 km s^{-1}.

This construction yields the general electron *internal* energy equation free of explicit body forces:

$$nU_r\left[kT_e\frac{d\ln(nT_e^{-3/2})}{dr} - \mathrm{TF}_r\right] + S_{ep} = \nabla\cdot\boldsymbol{q}_e, , \quad (32)$$

with the TF, TF_r, and energy exchange term, S_{ep}, explicitly present. All terms, except TF_r, and the source term S_{ep} are those typically considered for the electrons in the fluid plasma, with S containing the collision rates of energy transfer (e.g., Hartle & Sturrock 1968; Chandran et al. 2011). The term TF_r (and parts of S_{ep} developed below) allow serious consideration of the $\mathrm{TF}_r > 0$; the term TF_r represents an enhanced *cooling* for the electrons, by locally pushing $\nabla\cdot\boldsymbol{q}_e$ to be *more* negative. The term S_{ep} contains exchange terms with the ions from all circumstances. The nonzero size of the TF leads to a new contribution to S, a *second-order ohmic source term*, for the electrons discussed below in Section 7.2. (If formal ordering had expunged or ignored the TF from consideration of the $\mathrm{TF}_r \to 0$, then S would revert to the usual *very small* collisional Coulomb energy exchange between electrons and ions at rest, W_{ep}^E, retained by Hartle & Sturrock (1968), which will be shown below to be much smaller than that energy exchanged caused by the TF.)

The ion momentum equation takes a form complementary to Equation (31):

$$MU_r\frac{dU_r}{dr} + \frac{1}{n}\frac{d(nk_B T_p)}{dr} = -e\frac{d\Phi_E}{dr} - \mathrm{TF}_r + M\frac{d\Phi_G}{dr}, \quad (33)$$

with the sign of the charge and TF reaction reversed from that in Equation (31). Here the electric field levitates the ions away from the Sun and the reaction pair of the TF moderates that levitation.

The corresponding internal energy equation for the protons becomes (in the approximation Equation (32))

$$nU_r\left[kT_p\frac{d\ln nT_p^{-3/2}}{dr} + \mathrm{TF}_r\right] - S_{ep} = \nabla\cdot\boldsymbol{q}_p. \quad (34)$$

This ion analog of Equation (32) has the sign of charges reversed from the electron version: the TF makes a positive contribution to $\nabla\cdot\boldsymbol{q}_p$ for the ions, while the contribution from S_{ep} (dominated by the TF ohmic term discussed in Section 7.2) implies a complementary sink term for the ions. Equations (32) and (34) illustrate the linkages between the internal energy of electrons and ions made possible by incorporating the TF. In

this way the consideration of the TF effects a *redistribution* of available internal energy from that possible in its absence.

When the ion and electron internal energy equations are added, the terms TF_r and S_{ep} in Equations (32) and (34) sum to zero, so that they do not appear in the total internal energy equation.

If the test of the solar wind model is to reproduce the temperature partition between ions and electrons (see Hartle & Sturrock 1968; Breech et al. 2009; Cranmer et al. 2009; Chandran et al. 2011), the corresponding, consistent, and correct TF *must* be included in the respective internal energy equations. Further, the practice of adopting an ad hoc moment heat law without specifying the attendant TF cannot be expected to predict the observed temperature partition of the ions and electrons; such assumptions have no guarantee that they are consistent with the $GOL_{\|}$ or zero current, or accordingly closed in a consistent theoretical manner. Neither can such incomplete descriptions be used to suggest that new model physics included is adequate (or not) because of these deficiencies.

7.2. $\mathbb{TF}$ and Second-order Ohmic Source

The source term S_{ep} in the electron energy variant of Equation (30) represents (i) exchange energy W^E_{ep} between ions to electrons modeled as Gaussians at rest in the center of mass frame, and (ii) a form of TF induced second-order ohmic heating, $S^{\mathbb{TF}}$, caused by the skewing of the velocity space in opposite directions along $\boldsymbol{B}$, accomplished against opposite drags produced by the ions on counterdrifting parts of the eVDF. The (ii) form is initiated by the quasi-neutral $E_{\|}$ that drives the overdamped thermal electrons to lag the ions, while the counter drift is a zero return current corollary response to $E_{\|}$ that initiated the skew (Scudder 2019b). Clearly the displacement of the thermal and suprathermals are opposed by ion drag, so the drag produces a frictional heating of both species, at rates determined by their respective component first-order Stokes drifts. Using the TF component drags, the $S^{\mathbb{TF}}$ source term becomes

$$\mathbb{S} = \frac{S^{\mathbb{TF}}}{neE_D w_e} = \left[(1-\delta)\frac{w_e}{w_c}\mathcal{M}_c\Psi_D(\mathcal{M}_c) + \delta\frac{w_e}{w_h}\mathcal{M}_h\Psi_D(\mathcal{M}_h)\right]. \quad (35)$$

The variation of $S^{\mathbb{TF}}(U)$ at 1 au from Equation (35) is shown in Figure 9 as the solid black line. The correction $W^E_{ep}(U)$ associated with the energy exchange between Gaussian

$$\frac{W^E_{ep}}{neE_D w_e} = -\frac{3m_e}{m_p}\frac{T_e - T_i}{T_e} \quad (36)$$

electrons and ions at rest in the ion frame has been added to $S^{\mathbb{TF}}(u)$ to plot the (indiscernible) red dashed–dotted line. This correction is more than 600 times smaller than the TF contribution to $S^{\mathbb{TF}}$, imperceptible in the graph that has the same units as those in Figure 10, and is an ignorable further correction to the energy equation. Thus, $S_e \simeq S^{\mathbb{TF}}$.

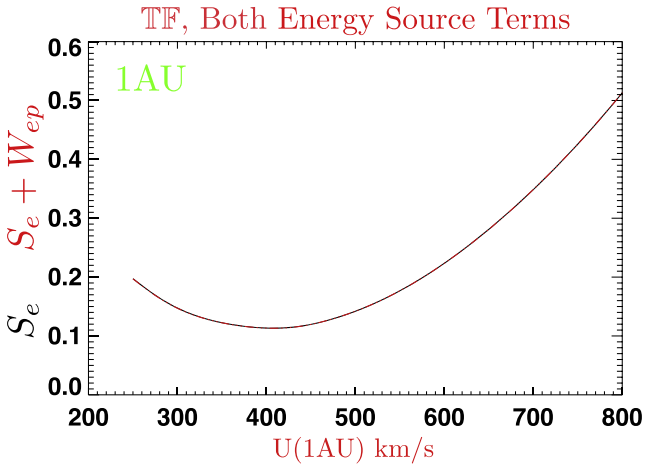

Figure 9. *Empirical* variation of $S^{\mathbb{TF}}$ (black) and $S^{\mathbb{TF}} + W^E_{ep}$ at 1 au (red dashed), virtually undetectable from the underlying black line for $S^{\mathbb{TF}}$ alone.

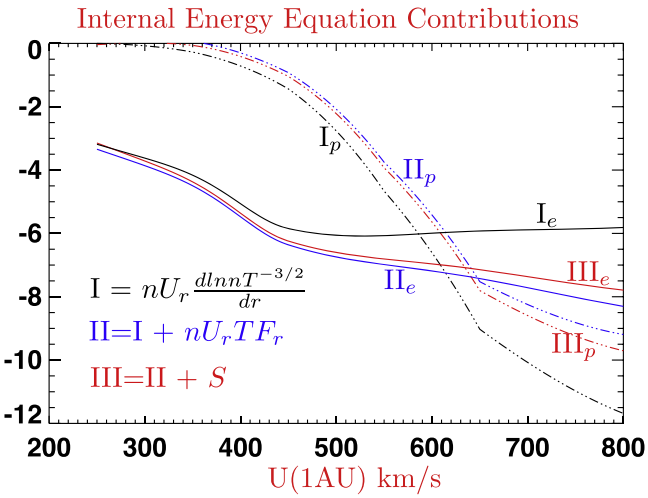

Figure 10. 1 au profiles vs. the solar wind speed of electron and ion terms in $\nabla \cdot \boldsymbol{q}_k = \mathrm{I}_k + \mathrm{II}_k + \mathrm{III}_k$. Vertical scale is linear and negative, indicative of cooling; larger absolute values imply faster cooling rates (depletions of internal energy). Note that the TF increases (decreases) the electron (ion) moduli of their respective, but still negative divergences.

8. $\mathbb{TF}$ Two-fluid Picture $\nabla \cdot q_j$ (1 au, U)

It is now possible to bring together the information required to illustrate the $\nabla \cdot \boldsymbol{q}_j$ variation with bulk speed at 1 au. Solar cycle-independent statistical profiles for the ions in the form of the Burlaga–Ogilvie relationship (Burlaga & Ogilvie 1970) $T_p(U)$ and radial power-law trends from Lopez & Freeman (1987) are used for the entropy terms for the ions in Equation (34), while the electron variability is taken from a recent Helios study (Scudder 2019c) and the TF profiles come from the above analysis.

Figure 10 illustrates the contributing profiles to $\nabla \cdot \boldsymbol{q}_j$ in three successive approximations: $\mathrm{III}_e = \nabla \cdot \boldsymbol{q}_e$ at 1 au and $\nabla \cdot \boldsymbol{q}_p = \mathrm{III}_p$ as a function of bulk speed determined using the same observed profile parameter variations for electrons used as in other figures in this paper. The III_j profiles are the suggested "observed" variations of $\nabla \cdot \boldsymbol{q}_j(U)$ possible. Of note is that despite the usual attempts to ignore $\nabla \cdot \boldsymbol{q}_p$ in modeling the solar wind heating problem (e.g., Breech et al. 2009; Cranmer et al. 2009), there is in these data considerable

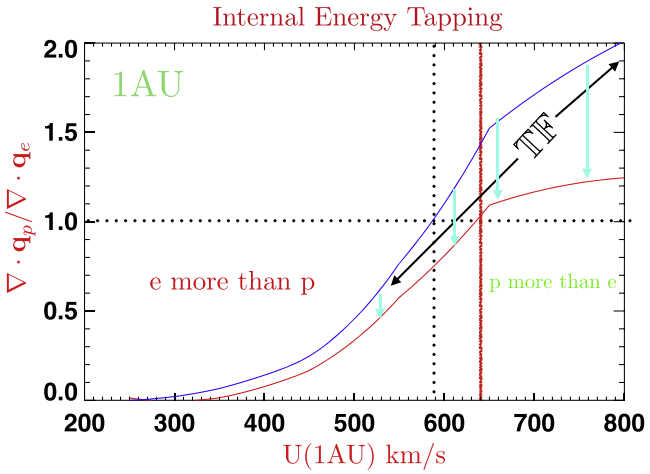

Figure 11. Comparison of inferred electron to ion cooling rates at 1 au as a function of bulk speed. The red line includes all effects of $TF_{\parallel}$ estimated from this paper; the blue line is the ratio of divergences ignoring the TF altogether as is common in the literature to date. For $U < 610\,\mathrm{km\,s^{-1}}$ electron cooling dominates with $TF_{\parallel} \neq 0$, while above this speed at 1 au ion cooling dominates.

evidence of negative ion heat divergence, with a sizable variation in its size with bulk speed; only the lowest speed winds are at all consistent with possibly having quasi-adiabatic behavior, a conclusion already reached (Scudder 2015).

The curves labeled as I_j are the baseline entropy terms of the divergences, assuming $\mathbb{TF}_{\parallel} = 0$, $S = 0$, while the curves labeled II_j reflect the revised profile of $\nabla \cdot \boldsymbol{q}_j$ when the inferred TF is included, but the second-order ohmic heating of electrons is ignored.

Figure 10 shows that the dominant TF effect on the size of $\nabla \cdot \boldsymbol{q}_j$ is well estimated by the curves labeled II_j, and only marginally improved by the second-order ohmic source term S. However, it is hard to evaluate the cumulative importance of the solar wind radial profiles of these modifications to the rates, since they will scale with the unknown radial variations of TF and S_e over r of each of these new terms as well as a solution with the *appropriate closure*.

A sense of the impact of the TF using the available 1 au data can be seen in Figure 11, where the ratio of ion-to-electron divergence versus wind speed are shown with (solid) and without (dashed) contributions from the TF. For wind speeds below the transition at $610\,\mathrm{km\,s^{-1}}$ ($585\,\mathrm{km\,s^{-1}}$), electron cooling dominates ion cooling with (without) the TF contributions. Since the TF importance grows with wind speed, the comparison of these cooling rates differ by factors of 2 above these transition speeds, with ions cooling nearly twice as fast as the electrons if the effects of the TF are ignored. From this point of view the high-speed wind is characterized by the onset of strong TF effects that enhance the levitation of ions, moderate the rates of cooling of electrons relative to ions, in stark contrast to the implications from the ion internal energy content alone (I_p/I_e profiles dashed) that without TF effects are cooling twice as fast as the electrons, whereas with the TF effects their cooling rates have more nearly equilibrated as the bulk speed increases.

9. Summary

The TF is an omnipresent, numerically important frictional force in any heat-conducting plasma that is mass asymmetric, such as the hydrogenic solar wind. It remains nonzero even when the plasma supports no current, as in the customary multifluid plasma models of astrophysics with a common flow velocity.

The TF has been demonstrated to be measurable on a single spacecraft in the solar wind and to play a significant role in parallel force balance required to achieve a fluid model for that plasma. The finite Knudsen number regime of the solar wind is typical of plasmas found in astrophysics.

The dimensionless TF is proved to always be parallel to the dimensionless electron heat flux; with observables they are demonstrated to be 1–1 functions of one another.

The dimensionless TF has been shown in the solar wind to have increasing importance in the high-speed solar wind, and to be inversely dependent on the size of the local Coulomb electron–proton collision frequency.

The size of the TF represents a competition between the Coulomb collision rate that when increased tries to reduce its size and the parallel electric field that is the source of the skewness of the electron distribution function. This competition is won by the electric field for typical solar wind conditions above $400\,\mathrm{km\,s^{-1}}$.

The size of the TF and its velocity space support are pivotal to obtaining a physical heat law closure that can confidently predict the properties of the plasma *and* the partition of internal energy among its constituents.

Theoretically the TF is shown to change the structure of the internal energy equations of the constituent species. The size of these energy exchanges between species is controlled by the electron heat flow which is a 1–1 function of the TF.

Since the TF and heat flow are physically tandem, one cannot be logically presumed present without the other. The extant practice in astrophysical fluid modeling of choosing ad hoc moment heat laws for closure without a physically consistent TF recipe vacates all physical predictions from such a model about the separate species temperature profiles.

The helpful comments of the referee are acknowledged. It is a pleasure to thank C. Salem and M. Pulupa for sharing results in advance of their publication (Salem & Pulupa 2019). Support provided by NASA grant 80NSSC19K1114.

ORCID iDs

J. D. Scudder https://orcid.org/0000-0001-7975-5630

References

Balescu, R. 1988, Transport Processes in Plasmas, Vol. I (Amsterdam: North-Holland)
Braginskii, S. I. 1965, RvPP, 1, 205
Breech, B., Matthaeus, W. H., Cranmer, S. R., Kasper, J. C., & Oughton, S. 2009, JGR, 114, A09103
Burlaga, L. F., & Ogilvie, K. W. 1970, ApJ, 159, 659
Chandran, B., Dennis, T., Quaetert, E., & Bale, S. D. 2011, ApJ, 743, 197C
Chapman, S. 1916, Philos. Trans. R. Soc. A, 216, 279
Cranmer, S. R., Mattheus, W. H., Breech, B. A., & Kasper, J. C. 2009, ApJ, 702, 1604
Dreicer, H. 1959, PhRv, 115, 238
Dreicer, H. 1960, PhRv, 117, 329
Enskog, D. 1917, Inaugural dissertation, Uppsala
Feldman, W. C., Asbridge, J. R., Bame, S. J., Montgomery, M. D., & Gary, S. P. 1975, JGR, 80, 4181
Ferziger, J. H., & Kaper, H. G. 1972, Mathematical Theory of Transport Processes in Gases (Amsterdam: North-Holland)
Fitzpatrick, R. 2014, Plasma Physics, an Introduction (Boca Raton, FL: CRC Press)
Forslund, D. W. 1970, JGR, 75, 17

Gary, P. S., Feldman, W. C., Forslund, D. W., & Montgomery, M. D. 1975, GeoRL, 2, 79
Hartle, R. E., & Sturrock, P. A. 1968, ApJ, 151, 1153
Issautier, K., Meyer-Vernet, N., Moncuquet, M., & Hoang, S. 1998, JGR, 103, 1969
Lemaire, J., & Scherer, M. 1973, RvGSP, 11, 427
Lopez, R., & Freeman, J. 1987, JGR, 92, 697
Meyer-Vernet, N. 2007, Basics of the Solar Wind (Cambride: Cambridge Univ. Press), 252
Montgomery, M. D., Bame, S. J., & Hundhausen, A. J. 1968, JGR, 116, 4999
Pulupa, M., Bale, S. D., Salem, C., & Horaties, K. 2014, JGR, 119, 647
Rosenbluth, M. N., MacDonald, W. M., & Judd, D. L. 1957, PhRv, 107, 1
Rossi, B., & Olbert, S. 1970, Introduction to the Physics of Space (New York: McGraw Hill)
Salem, C., & Pulupa, M. 2019, A&A, submitted
Scudder, J. D. 1996, JGR, 101, 11039
Scudder, J. D. 2015, ApJ, 809, 126S
Scudder, J. D. 2019a, ApJ, submitted
Scudder, J. D. 2019b, ApJ, submitted
Scudder, J. D. 2019c, JGR, submitted
Scudder, J. D., & Karimabadi, H. 2013, ApJ, 770, 26
Spitzer, L. J. 1965, The Physics of Fully Ionized Plasmas (New York: Wiley-Interscience)
Spitzer, L. J., & Härm, R. 1953, PhRv, 89, 977